Enhanced tunneling electroresistance effects in HfZrO-based ferroelectric tunnel junctions by high-pressure nitrogen annealing

Youngin Goh, and Sanghun Jeon

Citation: Appl. Phys. Lett. **113**, 052905 (2018); doi: 10.1063/1.5040031
View online: https://doi.org/10.1063/1.5040031
View Table of Contents: http://aip.scitation.org/toc/apl/113/5
Published by the American Institute of Physics

Articles you may be interested in

Tunneling current in HfO_2 and $Hf_{0.5}Zr_{0.5}O_2$-based ferroelectric tunnel junction
Journal of Applied Physics **123**, 094501 (2018); 10.1063/1.5016823

Evolution of ferroelectric HfO_2 in ultrathin region down to 3 nm
Applied Physics Letters **112**, 102902 (2018); 10.1063/1.5017094

Silicon doped hafnium oxide (HSO) and hafnium zirconium oxide (HZO) based FeFET: A material relation to device physics
Applied Physics Letters **112**, 222903 (2018); 10.1063/1.5029324

Ferroelectricity in hafnium oxide thin films
Applied Physics Letters **99**, 102903 (2011); 10.1063/1.3634052

Effect of film thickness on the ferroelectric and dielectric properties of low-temperature (400 °C) $Hf_{0.5}Zr_{0.5}O_2$ films
Applied Physics Letters **112**, 172902 (2018); 10.1063/1.5026715

Robust ferroelectricity in epitaxial $Hf_{1/2}Zr_{1/2}O_2$ thin films
Applied Physics Letters **113**, 082902 (2018); 10.1063/1.5041715

MMR TECHNOLOGIES
THE WORLD'S RESOURCE FOR VARIABLE TEMPERATURE SOLID STATE CHARACTERIZATION
WWW.MMR-TECH.COM
Optical Studies Systems
Seebeck Studies Systems
Microprobe Stations
Hall Effect Study Systems and Magnets

Reuse of AIP Publishing content is subject to the terms at: https://publishing.aip.org/authors/rights-and-permissions. Downloaded to: 143.248.173.16 on 18 November 2018, At: 17:23

APPLIED PHYSICS LETTERS **113**, 052905 (2018)

Enhanced tunneling electroresistance effects in HfZrO-based ferroelectric tunnel junctions by high-pressure nitrogen annealing

Youngin Goh[1] and Sanghun Jeon[2,a)]
[1]*Department of Applied Physics, Korea University, 2511 Sejongro, Sejong 339-700, South Korea*
[2]*School of Electrical Engineering, Korea Advanced Institute of Science and Technology, 291 Daehakro, Yuseong-gu, Daejeon 34141, South Korea*

(Received 14 May 2018; accepted 20 July 2018; published online 2 August 2018)

Greatly improved ferroelectricity with an excellent remanent polarization of 20 μC/cm^2 and enhanced tunneling electroresistance (TER) were achieved with TiN/HfZrO(HZO)/p-type Ge ferroelectric tunnel junctions (FTJs) annealed at a high pressure of 200 atmosphere (atm.). We found that the enhanced ferroelectric characteristics can be ascribed to the effective formation of an orthorhombic phase at high pressures. This was verified by the combined study of grazing angle incidence X-ray diffraction, transmission electron microscopy, and hysteresis polarization curve analyses. In addition, using pulse switching measurements, we quantitatively evaluated the interfacial paraelectric capacitance (C_i) of HZO FTJs according to the annealing temperature. HZO films annealed at 550 °C and 200 atm. exhibited an excellent TER effect ratio of 20 due to the extra paraelectric layer between the ferroelectric layer and the bottom electrode and a relatively high remanent polarization. *Published by AIP Publishing.* https://doi.org/10.1063/1.5040031

Ferroelectric materials with perovskite structures, such as Pb(Zr, Ti)O_3, $BaTiO_3$, $SrBi_2Ta_2O_9$, and (K,Na)NbO_3, are widely studied in low-power non-volatile memory devices due to their switchable polarization under an applied electric field.[1,2] Of the various applications possible, ferroelectric tunnel junctions (FTJs) are considered as prospective candidates for the fabrication of next-generation non-volatile memory devices.[3–5] Perovskite-based conventional FTJs, which were first suggested by Esaki in 1971, are composed of an ultra-thin ferroelectric barrier inserted between two electrodes.[6] Because the barrier thickness is approximately a few nanometers, quantum mechanical tunneling can occur through the ferroelectric barrier.[7] Tunneling probability is associated with an effective barrier height and width, which are modulated according to the ferroelectric polarization direction, generating two or multi-level electrical resistance states. These give rise to the so-called tunneling electroresistance (TER) effect.[8] FTJs are non-volatile and exhibit nondestructive read-out characteristics, combining the advantages of fast read/write speed, reliability with scalability, and simplicity of manufacturing.[9–11] However, perovskite-based FTJs suffer from poor CMOS process compatibility due to the poor interface with silicon substrates. In addition, their low band gap (3–4 eV) limits scaling due to the leakage of current from the low Schottky barrier when forming a junction with a metal layer.[12]

In 2011, a new type of ferroelectric based on fluorite-type HfO_2-based thin films emerged.[13] It has been proposed that hafnia ferroelectric materials allow us to solve the problems associated with conventional perovskite-type ferroelectrics. Compared to traditional perovskite materials, HfO_2-based ferroelectrics offer many advantages including low processing temperatures (~450 °C), excellent compatibility with the CMOS process, high band gaps (5–6 eV), and high dielectric constants.[14,15] However, HfO_2-based ferroelectric materials typically exhibit poor ferroelectricity and low remanent polarization (P_r), compared to the traditional perovskite ferroelectrics, thereby preventing achieving high tunneling electroresistance.[14,16,17] The ferroelectricity of HfO_2-based materials comes from the formation of a non-centrosymmetric $Pbc2_1$ orthorhombic phase (o-phase), which is not thermodynamically stable under normal process conditions.[18,19] Therefore, it is necessary to apply a moderate mechanical stress on the HfO_2 film during the crystallization to stabilize the $Pca2_1$ o-phase, thereby achieving excellent ferroelectricity.[20] In this study, we report the fabrication of a [TiN/$Hf_{0.5}Zr_{0.5}O_2$ (HZO)/p-type Ge] junction by high-pressure annealing (HPA) at 500, 550, and 600 °C, and the impact of high-pressure nitrogen annealing on the characteristics of HZO FTJs.

Metal/ferroelectric/semiconductor (MFS)-type FTJs with HZO films were fabricated as shown in Fig. 1(a). 8 nm-thick HZO thin films were deposited on a p-type Ge semiconductor substrate via atomic layer deposition (ALD) at a stage temperature of 300 °C using TEMAHf, TEMAZr and ozone as the precursors for Hf, Zr, and O, respectively. The growth rates per cycle were 0.98 Å/cycle and 1 Å/cycle for HfO_2 and ZrO_2, respectively. A TiN top electrode was deposited on the prepared HZO layer by DC sputtering, followed by a patterning procedure using a wet etchant of NH_4OH:H_2O_2:H_2O solution (1:2:5) at 70 °C. For the comparison study, the HZO films were crystallized at 500 °C for 30 s in a nitrogen environment by rapid thermal annealing (RTA; reference) and for high-pressure annealing (HPA) under 200 atmosphere (atm) pressure for 30 min. In addition, to optimize the annealing conditions, we conducted HPA at various temperatures in the range of 500–600 °C. Figure 2(b) shows a schematic of the high-pressure annealing equipment used in this study. A high pressure is generated by injecting N_2 gas into a sealed chamber and raising the temperature.

a)Author to whom correspondence should be addressed: jeonsh@kaist.ac.kr

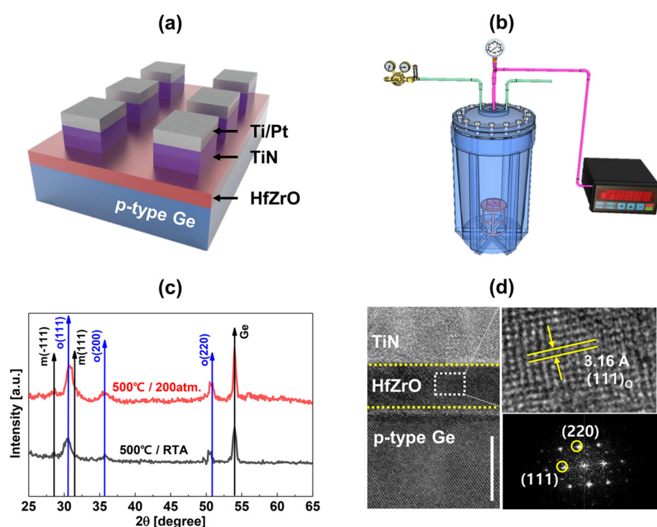

FIG. 1. (a) Schematic of the TiN/HZO/p-type Ge device structure. (b) Schematic of the high-pressure annealing equipment. (c) GIXRD patterns of the HZO films subjected to HPA and RTA. (d) Cross-sectional high-resolution transmission electron microscopy image and the FFT image of HZO-based FTJ with 500 °C HPA.

We employed a glancing incidence X-ray diffraction system (GIXRD; Rigaku, SmartLab) and a high-resolution transmission electron microscope (HRTEM; Titan) in the cross-sectional mode to understand the structure and ferroelectric properties of the HZO films. In addition, the electrical performance of the device was analyzed by polarization-electric field (P-E) hysteresis curves measured using a ferroelectric tester (Radiant Technologies, Precision LC II). Typical resistive switching was demonstrated in terms of the hysteretic current-voltage characteristics of the FTJs at a 0.2 V read voltage using a parameter analyzer (Agilent B1500). We also investigated the electrical switching kinetics of the FTJs by pulse-switching technique using a parameter analyzer (Agilent B1500).

In order to analyze the crystalline characteristics of the HZO thin films, we performed GIXRD and HRTEM. Figure 1(c) depicts the GIXRD spectra corresponding to the devices produced by RTA and HPA at 500 °C in the 2θ range 25°–65°. The diffraction peaks corresponding to the (111), (200), and (220) planes of the non-centrosymmetric o-phase, which are responsible for the ferroelectricity of HZO films, could be clearly detected in the diffraction patterns of both the devices. In fact, because of structural similarities, the peak near $2\theta \sim 30.5°$, which was mentioned as the (111) peak of the o-phase, was then better assigned as the mixture of (101) of the t-phase and (111) of the o-phase. The difference between the GIXRD patterns of the HZO films subjected to RTA and HPA lies in the difference in the relative ratios of the orthorhombic and monoclinic phases. In the case of the HZO film subjected to HPA, the relative peak area of orthorhombic and monoclinic phases exhibited a high ratio, indicating the formation of a highly stabilized o-phase, in comparison to conventional RTA. Figure 1(d) shows the HRTEM and fast-Fourier transformation (FFT) of the lattice, which can be used to further validate that exact structural phase of the HZO film subjected to HPA. The lattice fringes of the HZO layers on the p-type Ge substrate shown in the yellow box in Fig. 1(d) represent the o(111) plane with an interplanar distance (d) of 3.16 Å. In the FFT images, the diffraction points indicated by yellow circles matched with the o(111) planes, which suggests that film crystallization occurred effectively under high-pressure conditions. Figures 2(a) and 2(b) show the polarization-electric field (P-E) hysteresis curves of the HZO films crystallized during RTA and HPA, respectively, at 3, 4, and 5 MV/cm. As for the HZO film subjected to HPA, stable P-E hysteresis can be observed with a large P_r value of 20 μC/cm^2 and a steep slope of the P-E curve near coercive field (E_c). Furthermore, the E_c value significantly decreased compared to the HZO film subjected to RTA [Fig. 2(c)]. In previous works, Yu *et al.*[21] and Park *et al.*[22] observed that an in-plane tensile stress can transform the c-axis of the tetragonal phase (t-phase) into the a-axis of the o-phase activating the formation of ferroelectric o-phase. In addition, Kim *et al.* quantitatively investigated the influence of high-pressure nitrogen annealing on the ferroelectric characteristics of HfO_2-based capacitors confirming that enhancements arise from phase transitions to the o-phase from the t-phase.[23] As shown in Fig. 1(c), as the annealing pressure increases, the inter-planar distance of (111) planes (d_{111}) decreases, which could be calculated from shift of the t(111) or o(111) diffraction peak to higher angles. This result is involved in the in-plane tensile stress during the annealing process in HZO films and it can influence the phase transition from the t-phase to the o-phase, which is consistent with the previous study.

In order to systematically analyze the effect of annealing temperature on the crystal structure and the ferroelectric properties of HZO films; we prepared HZO-based FTJ devices crystallized via HPA at different temperatures (500, 550, and 600 °C). The P-E hysteresis curves of each of the devices are exhibited in Figs. 3(a)–3(c). As shown in Figs. 3(a) and 3(b), for the device with the HZO film annealed at 500 °C and 550 °C under high-pressure, nearly similar and stable P-E hysteresis properties were observed with a maximum P_r value of 19–20 μC/cm^2, indicating that both devices have similar crystallinity to contribute to the formation of ferroelectric materials. However, the HZO device formed by 550 °C HPA exhibits a lower E_c value and a more gradual

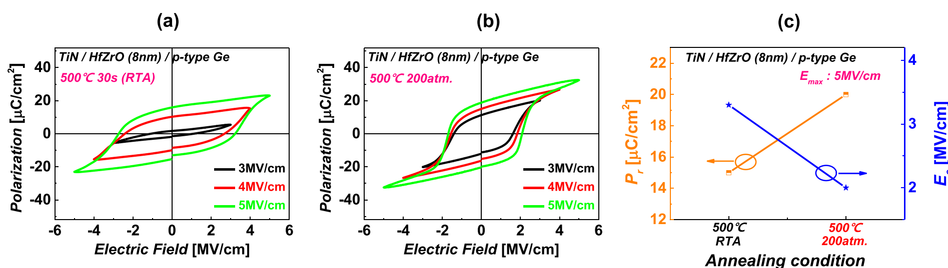

FIG. 2. P-E hysteresis characteristics of HZO-based FTJs subjected to (a) 500 °C RTA and (b) 500 °C HPA. (c) Comparison of the P_r and E_c values of HZO-based FTJs subjected to 500 °C RTA and 500 °C HPA.

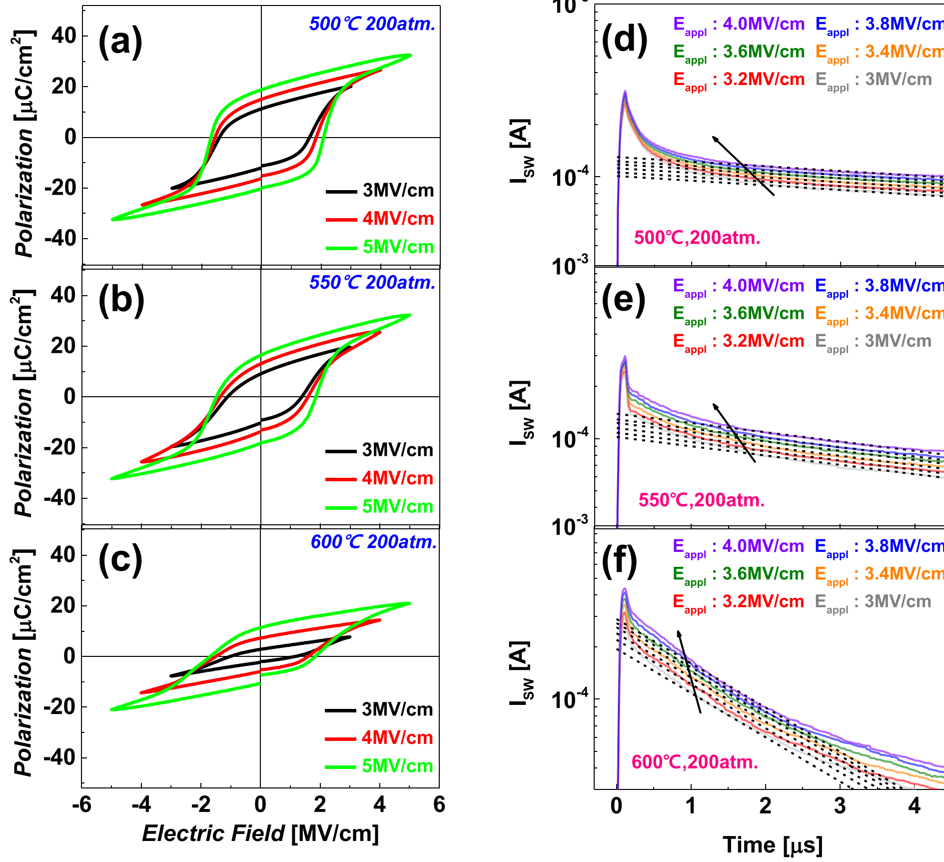

FIG. 3. P-E hysteresis characteristics of HZO-based FTJs subjected to annealing at (a) 500 °C and 200 atm, (b) 550 °C and 200 atm, and (c) 600 °C and 200 atm. Transient domain switching current vs time curves of HZO-based FTJs annealed at (d) 500 °C and 200 atm, (e) 550 °C and 200 atm, and (f) 600 °C and 200 atm.

slope at E_c compared to that of 500 °C HPA. On the other hand, the HZO device formed at 600 °C HPA exhibited weak ferroelectricity and a gradual slope at E_c which is reflected in the relatively low P_r value of ∼10 μC/cm^2. In fact, HZO films are mixture grains of ferroelectric and non-ferroelectric phases. At annealing temperatures over 600 °C, the film is mostly crystallized into a non-ferroelectric phase, especially in interfacial layer. Due to the non-ferroelectric phase, the effective electric field applied to the ferroelectric phase decreased indicating decreasing P_r and a gradual slope at E_c.

To examine the ferroelectric and non-ferroelectric domain compositions of the HZO films, we analyzed the switching kinetics of three devices using a short-pulse switching technique.[24] Initially, we applied a negative write pulse of 4 MV/cm to induce polarization in the HZO films in one direction and then the switching current was evaluated while applying positive pulses of varying magnitude from 3 MV/cm to 4 MV/cm. Figures 3(d)–3(f) show the transient switching current of HZO-based FTJ devices annealed at 500, 550, and 600 °C at high pressures, respectively. In accordance with the polarization reversal theory, the domain switching current (I_{SW}) is calculated using the following equation:

$$I_{SW}(t) = I^0_{SW} e^{\frac{t-t_0}{R_L C_i}} \quad (t_0 < t < t_{sw}), \tag{1}$$

where I^0_{sw} is the starting current of the switching process, t_0 is the switching starting time, R_L is the total possible resistance, C_i is the interfacial capacitance and t_{sw} is the time when the switching process is finished. This theory fundamentally states that when the switching process starts, marked by the arrow in Figs. 3(d)–3(f), a switching current flows linearly through the ferroelectric layer, which indicates that the ferroelectric layer performs like a resistor. Then, I^0_{SW} can be described as

$$I^0_{SW} = \frac{(E_a - E_c)t_f}{R_L}, \tag{2}$$

where E_a, E_0, and t_f are the applied field, the coercive electric field, and the HZO film thickness, respectively. Therefore, E_c and R_L can be obtained from the plot of I^0_{SW} as a function of E_a by extracting the intercept of the x-axis and the slope of the graph, as shown in Fig. 4(a). Finally, C_i can also be extracted from the $I_{sw}(t)$ graph by substituting the R_L value in Eq. (1). As shown in Fig. 4(b), the decrease in the C_i value with an increase in the annealing temperature indicates the increase in interfacial non-ferroelectric t-phases due to high temperatures. This is consistent with the decrease in the P_r

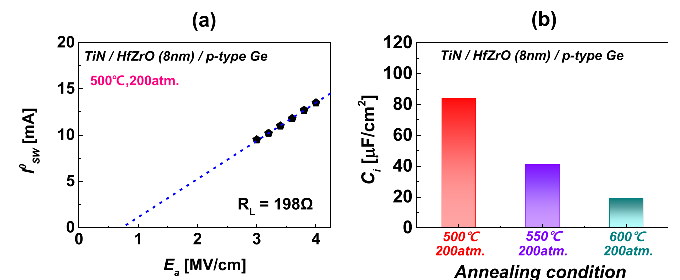

FIG. 4. (a) Switching start current as a function of the applied electric field. (b) Extracted C_i values of the HZO-based FTJs at different annealing temperatures.

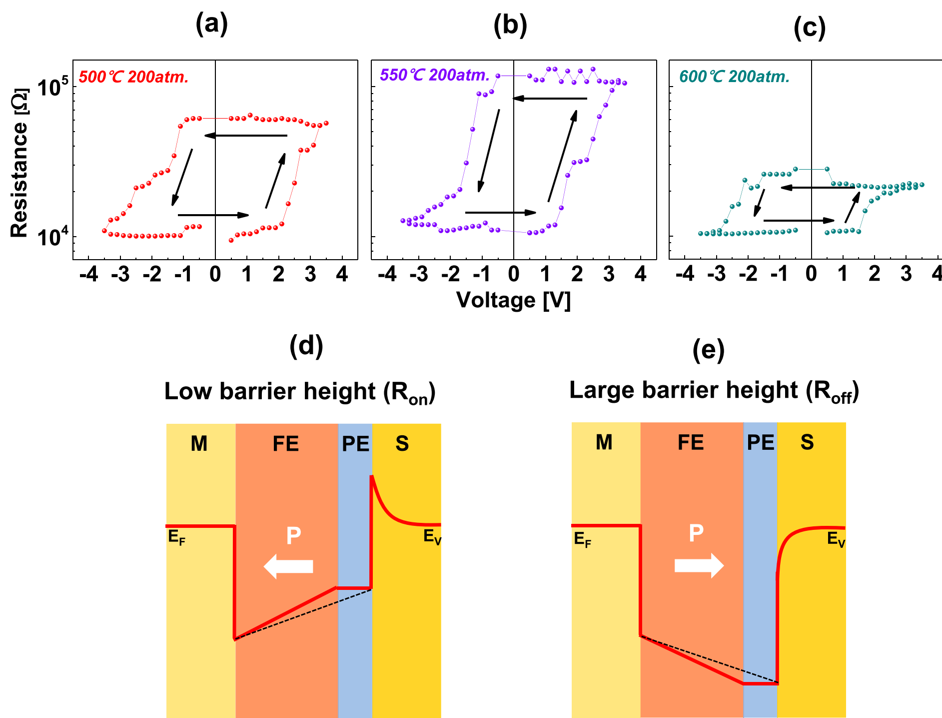

FIG. 5. (a) Resistance-voltage hysteresis loops of HZO-based FTJs annealed at (a) 500 °C, (b) 550 °C, and (c) 600 °C. Band diagrams of FJT junctions with interfacial non-ferroelectric layers developed according to the polarization direction: (d) ON state and (e) OFF state.

value with increasing annealing temperature. Therefore, it can be concluded that a high-temperature annealing process on a hafnia device induces interfacial non-ferroelectric t-phases and weak ferroelectricity.

To confirm the influence of annealing temperature on tunneling, we analyzed the resistance-write voltage (R-V) curve reading at 0.2 V. Figures 5(a)–5(c) show the electrical resistance switching of the three devices at different annealing temperatures (500, 550 and 600 °C). The TER effects were apparent in all three HZO-based FTJs; a maximum TER value of 10 was obtained with the HZO-based FTJ annealed at 550 °C in a HP environment. Interestingly, devices with 500 and 550 °C HPA have a similar Pr value, but the TER effect is significantly improved in devices with 550 °C HPA. Comparing the FTJ devices annealed at 500 °C and 550 °C as seen in Figs. 5(a) and 5(b), the HZO FTJ devices with 550 °C HPA have an extra interfacial non-ferroelectric layer which makes an additional parameter for adjusting the tunneling barrier.[25] As schematically described in Figs. 5(d) and 5(e), an interfacial non-ferroelectric is a paraelectric layer which has a relatively high dielectric constant resulting in unchanged potential profiles, depending on polarization switching. As a result, for a fixed total film thickness, the HZO-based FTJ annealed by 550 °C HPA certainly has a lower (higher) potential barrier height in the ON (OFF) state than the HZO-based FTJ annealed at 500 °C. On the other hand, despite the formation of a non-ferroelectric layer at the interface, the HZO-based FTJ annealed at 600 °C has a low TER value due to weak ferroelectricity as shown in Fig. 5(c). Basically, tunneling probability depends not only on the barrier height but also on remanent polarization, which determines the magnitude of ferroelectric bound charges and accordingly modulates the potential profiles. The low TER value of the HZO-based FTJ produced by HPA at 600 °C is consistent with the previous results.

In this study, we investigated a CMOS-compatible non-volatile HZO-based FTJ crystallized by high-pressure nitrogen annealing. The influence of annealing pressure on the ferroelectricity of HZO films was verified by GIXRD, HRTEM, and P-E hysteresis curve analyses. A large proportion of the ferroelectric o-phase and an improved remanent polarization were observed under high-pressure nitrogen annealing conditions when compared to HZO films subjected to RTA due to effective phase transition from the t-phase to the o-phase under in-plane tensile stress. Furthermore, based on short pulse measurements, we analyzed the ferroelectric and non-ferroelectric domain distributions in HZO-based FTJs according to the annealing temperature. It could be confirmed that as the annealing temperature increases, an interfacial non-ferroelectric layer is formed, resulting in a decrease in the interface capacitance value. By modulating this interfacial paraelectric layer in an appropriate manner, we could obtain a maximum TER value of 10 with the HZO-based FTJ subjected to HPA at 550 °C.

This work was supported by the Samsung Research Funding Center of Samsung Electronics under Project No. SRFC-TA1703-01.

[1]P. Muralt and J. Micromech, Microengineering **10**, 136 (2000).
[2]Y. Goh and S. Jeon, Nanotechnology **29**, 335201 (2018).
[3]A. Chanthbouala, A. Crassous, V. Garcia, K. Bouzehouane, S. Fusil, X. Moya, J. Allibe, B. Dlubak, J. Grollier, S. Xavier, C. Deranlot, A. Moshar, R. Proksch, N. D. Mathur, M. Bibes, and A. Barthelemy, Nat. Nanotechnol. **7**, 101 (2012).
[4]M. Y. Zhuravlev, R. F. Sabirianov, S. S. Jaswal, and E. Y. Tsymbal, Phys. Rev. Lett. **94**, 246802 (2005).
[5]H. Kohlstedt, N. A. Pertsev, J. R. Contreras, and R. Waser, Phys. Rev. B **72**, 125341 (2005).
[6]A. L. Esaki, R. B. Laibowits, and P. J. Stiles, IBM Tech. Discl. Bull. **13**, 114 (1971).

[7]E. Y. Tsymbal, A. Gruverman, V. Garcia, M. Bibes, and A. Barthélémy, MRS Bull. **37**, 138 (2012).
[8]E. Y. Tsymbal and H. Kohlstedt, Science **313**, 181 (2006).
[9]R. Waser and M. Aono, Nat. Mater. **6**, 833 (2007).
[10]V. Garcia and M. Bibes, Nat. Commun. **5**, 4289 (2014).
[11]Z. Wen, C. Li, D. Wu, A. Li, and N. Ming, Nat. Mater. **12**, 617 (2013).
[12]M. H. Park, H. J. Kim, Y. J. Kim, W. Lee, T. Moon, and C. S. Hwang, Appl. Phys. Lett. **102**, 242905 (2013).
[13]J. Müller, T. S. Böscke, D. Bräuhaus, U. Schröder, U. Böttger, J. Sundqvist, P. Kücher, T. Mikolajick, and L. Frey, Appl. Phys. Lett. **99**, 112901 (2011).
[14]A. Chernikova, M. Kozodaev, A. Markeev, D. Negrov, M. Spiridonov, S. Zarubin, O. Bak, P. Buragohain, H. Lu, E. Suvorova, A. Gruverman, and A. Zenkevich, ACS Appl. Mater. Interfaces **8**, 7232 (2016).
[15]M. H. Park, J. J. Kim, Y. J. Kim, W. Lee, H. K. Kim, and C. S. Hwang, Appl. Phys. Lett. **102**, 112914 (2013).
[16]F. Ambriz-Vargas, G. Kolhatkar, M. Broyer, A. Hadj-Youssef, R. Nouar, A. Sarkissian, R. Thomas, C. Gomez-Yáñez, M. A. Gauthier, and A. Ruediger, ACS Appl. Mater. Interfaces **9**, 13262–13268 (2017).
[17]F. Ambriz-Vargas, G. Kolhatkar, R. Thomas, R. Nouar, A. Sarkissian, C. Gomez-Yáñez, M. A. Gauthier, and A. Ruediger, Appl. Phys. Lett. **110**, 093106 (2017).
[18]S. Mueller, J. Mueller, A. Singh, S. Riedel, J. Sundqvist, U. Schroeder, and T. Mikolajick, Adv. Funct. Mater. **22**, 2412 (2012).
[19]J. Müller, U. Schröder, T. S. Böscke, I. Müller, U. Böttger, L. Wilde, J. Sundqvist, M. Lemberger, P. Köcher, T. Mikolajick, and L. Frey, J. Appl. Phys. **110**, 114113 (2011).
[20]M. H. Park, H. J. Kim, Y. J. Kim, W. Lee, T. Moon, K. D. Kim, and C. S. Hwang, Appl. Phys. Lett. **105**, 072902 (2014).
[21]H. Yu, C. C. Cung, N. Shewmon, S. Ho, J. H. Carpenter, R. Larrabee, T. Sun, J. L. Jones, H. Ade, B. T. O'Connor, and F. So, Adv. Mater. **27**, 1700461 (2017).
[22]T. Kim and S. Jeon, IEEE Trans. Elect. Dev. **65**, 1771 (2018).
[23]T. Kim, J. Park, B. H. Cheong, and S. Jeon, Appl. Phys. Lett. **112**, 092906 (2018).
[24]H. J. Kim, M. H. Park, Y. J. Kim, Y. H. Lee, T. Moon, K. D. Kim, S. D. Hyun, and C. S. Hwang, Nanoscale **8**, 1383 (2016).
[25]L. Wang, M. R. Cho, Y. J. Sin, J. R. Kim, S. Das, J. G. Yoon, J. S. Chung, and T. W. Noh, Nano Lett. **16**, 3911 (2016).